Schweizerischer Erdbebendienst
Service Sismologique Suisse
Servizio Sismico Svizzero
Swiss Seismological Service

ETH zürich

SITE CHARACTERIZATION REPORT

SMOE: Moudon (VD) - Ecole

Clotaire Michel, Manuel Hobiger, Donat Fäh

Last Modification: 18th November, 2016

Schweizerischer Erdbebendienst (SED)
Service Sismologique Suisse
Servizio Sismico Svizzero
Servizi da Terratrembels Svizzer

ETH Zurich
Sonneggstrasse 5
8092 Zurich
Schweiz
clotaire@sed.ethz.ch

Contents

Summary

The new station SMOE was installed in the town of Moudon (VD) within the school area and the installation site has been characterized. We performed passive seismic array measurements that successfully allowed us to retrieve the 1D velocity profile at the station site. The soft sediment cover (old alluvia and moraine) is about 15 m thick with a low velocity over the 2-3 first meters and of about 530 m/s below. The rock below (Upper Marine Molasse) has a velocity of about 1200 m/s. Another noticeable increase of velocity is found at about 70 m depth. We also studied the distribution of the sediment cover in the town using single station measurements (H/V technique) and borehole data. $V_{s,30}$ is 582 m/s and the site corresponds to ground type B in the Eurocode 8 (CEN, 2004) and type E in the SIA261 (SIA, 2014). The theoretical 1D SH transfer function computed from the inverted profiles shows an amplification of a factor 2 to 3 at the resonance frequency of the soft sediment cover at about 10 Hz.

1 Introduction

In the framework of the second phase of the Swiss Strong Motion Network (SSMNet) renewal project, a new installation in Moudon (VD), in the Etablissement secondaire of Moudon-Lucens was decided. It is located in the Broye valley (see Fig. 1), in hilly area of the Swiss foreland. The new station went operational on 11 March 2015.

Figure 1: Station SMOE (foreground) in the school area and view on the Broye valley towards East. Picture taken during the passive array measurement (orange boxes).

2 Geological setting

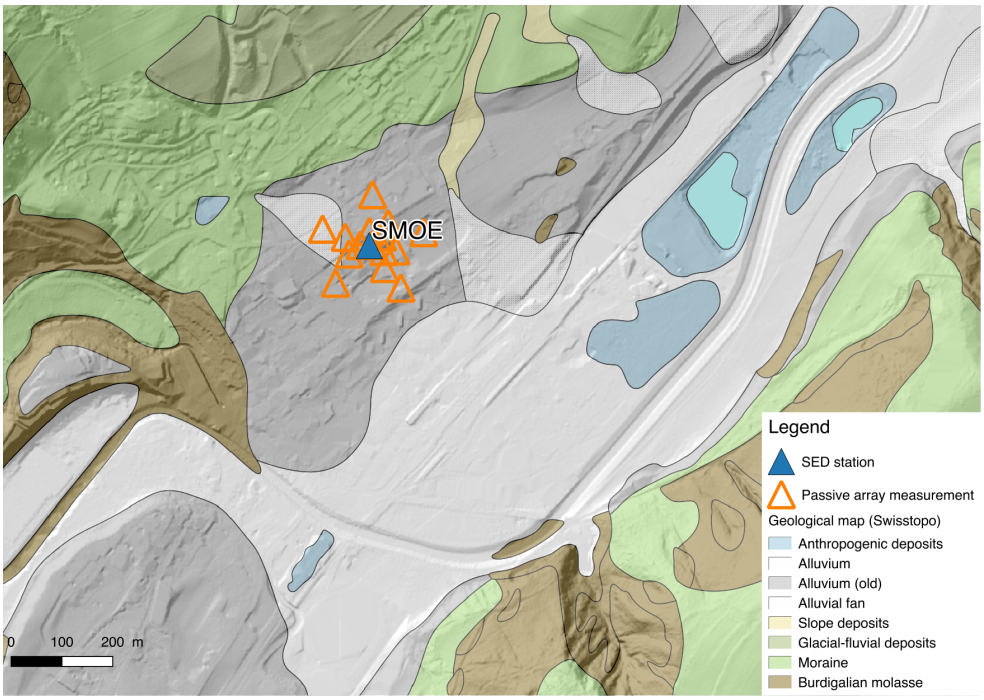

Figure 2: Geological map of the Broye valley in Moudon (Data: ©2016 swisstopo (JD100042)).

The site SMOE is located in the valley of the Broye river in the Swiss foreland (Fig. 2). The site has a slight slope towards the valley centre, with 15 m height difference between the top and the bottom of the array measurement. At the station site, one finds alluvium from the Broye river referenced as "old" in the geological map with respect to those in the central part of the valley. The thickness of the alluvium is 10.4 m according to the closest borehole in the school area, located 28 m away from SMOE. Other boreholes in the school area show at least 12 m of alluvia and did not reach the moraine.
According to another borehole in the school area, a thin layer of about 2.2 m of moraine is present below the alluvium. This moraine is present in thicker layers at other places of the valley and on the valley sides (Fig. 2). Considering the slope of the site, it is however difficult to predict accurately the thickness of the loose sediments.
Below the moraine, one reaches the sandstones of the Upper Marine Molasse (OMM) ("Couches de la Singine" in French, "Sense Schichten" in German) dated of Lower Burdigalian age (Miocene, Tertiary). The thickness of this layer, outcropping at many places in the valley (Fig. 2), is between 25 and 72 m according to boreholes in the area of SMOE station.
Below, one finds the marls and sandstones of the Lower Freshwater Molasse (USM) ("Molasse grise de Lausanne ") dated of Aquitanian age (Miocene, Tertiary). This layer is about 1500 m thick at this location. These conditions are representative of a large part of the city centre of Moudon, where the sediments can however reach 18 m in thickness and the moraine 9 m. Another part of the city lays directly on the Burdigalian Molasse rock (Fig. 2).
This site is classified as ground type E (SIA261) by the Federal Office for the Environment.

3 Site characterization using passive measurements

3.1 Measurements and data set

We investigated the local underground structure by passive seismic array measurements which took place on July 15th, 2016. The layout of the seismic arrays is shown in Fig. 3. Two configurations were used.
The parameters of both arrays are given in Table 1. For these measurements 12 Nanometrics Centaur dataloggers named NR42 to NR49 and NR52 to NR55 and 15 Lennartz 3C 5 s seismometers were available. Each datalogger can record on 2 ports A (channels EH1, EH2, EH3 for Z, N, E directions) and B (channels EH4, EH5, EH6 for Z, N, E directions). Time synchronization is ensured by GPS. The sensors were placed on a metal tripod, in a 15 cm deep hole, when possible, for better coupling with the ground.
The sensor coordinates were measured using a differential GPS device (Leica Viva GS10), including only a rover station and using the Real Time Kinematic technique provided by Swisstopo. It allows an absolute positioning with an accuracy better than 4 cm on the Swissgrid.

Table 1: List of the seismic array measurements in Moudon.

Array name	Number of sensors	Minimum interstation distance [m]	Aperture [m]	Recording time [min]
MOE1	15	10	100	125
MOE2	15	25	200	126

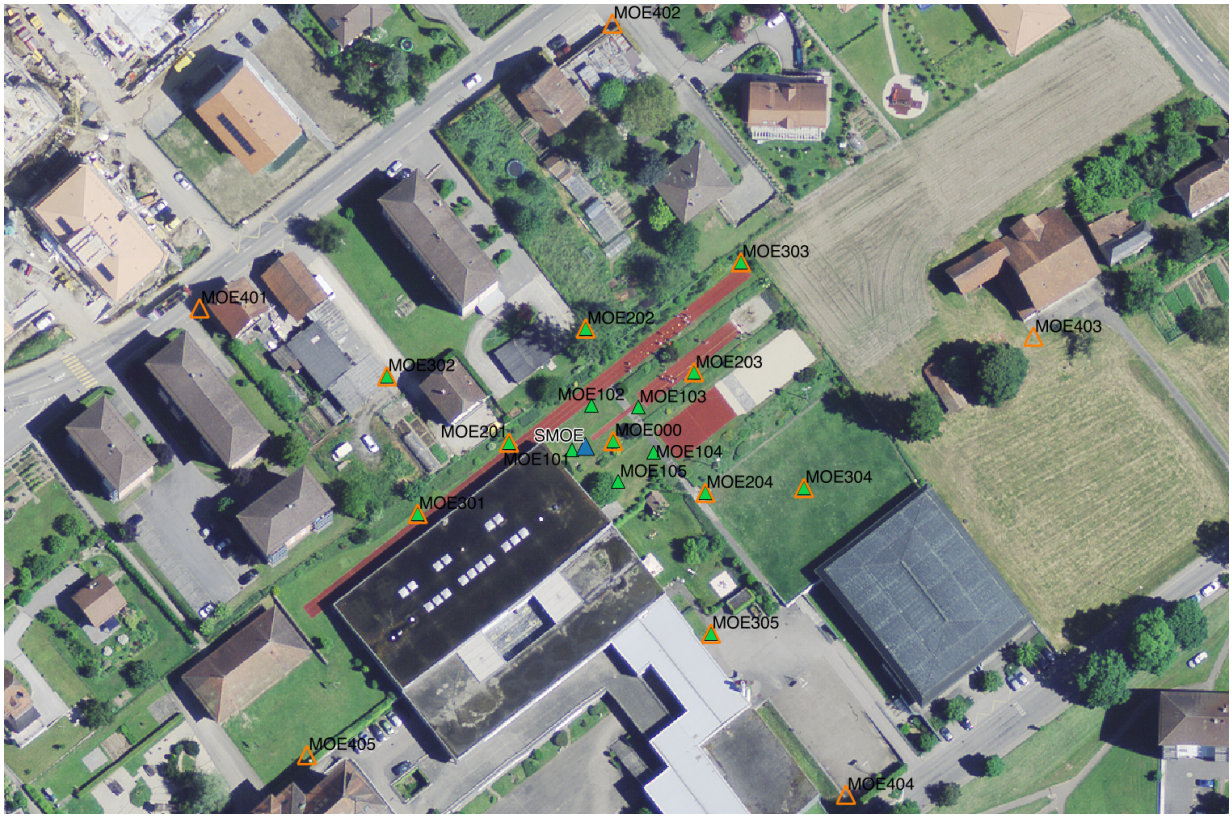

Figure 3: Layout of the array measurements at site SMOE.

The largest time windows were extracted, for which all the sensors of the array were correctly placed and the GPS synchronization was ensured. A strong disturbance at 0.73 Hz (damped but clear peak) in the vertical component can be noticed during the second configuration MOE2. The lawn has been mowed inside the array during the last 15 minutes of MOE1 and the first 15 minutes of MOE2.
Orientations of the sensors were checked by maximizing the correlation with the central station at low frequencies (Poggi et al., 2012b). Corrections lower that 10 ° were generally observed, although they reached 13 ° in MOE101, MOE301 and MOE305 and 21 ° in MOE404.

3.2 Single station measurements results

3.2.1 H/V curves

A strong difference between the H/V curves is noticed between MOE1 and MOE2 due to the disturbance at 0.73 Hz in the vertical component, resulting in a trough for the MOE2 H/V curves at this frequency. This said, all curves show a similar shape across the array below 4 Hz (Fig. 4). A wide peak can be observed at 0.65 Hz that was finally not interpreted as related to the geology because 1) on the long term measurement XMOU1 in the school building, although a small peak can be observed at 0.52 Hz (see Fig. 7), it is different in frequency, width and amplitude from what is observed in the array (Fig. 4) and 2) considering the retrieved velocity structure in section 4.1, such an interface would lie at several hundreds of meters depth (Fig. 17), within the very thick Lower Freshwater Molasse where no important velocity contrast is expected. Therefore, this bump may be related to the noise sources.
Another peak with variable frequency values is observed across the array and is interpreted as the resonance of the Quaternary sediments. Fig. 5 shows the distribution of the values of this peak, together with the results of a single station array campaign performed previously in the town. It varies between 2.3 Hz in the centre of the valley and 12 Hz close to the rock. Close to SMOE it is consistent, with values around 10 Hz. Its spatial distribution corresponds well to the surface geology of this small alluvial basin (Fig. 5). In this figure, the thickness of the Quaternary sediments from borehole data is also given and correlates well with the H/V frequency peak.

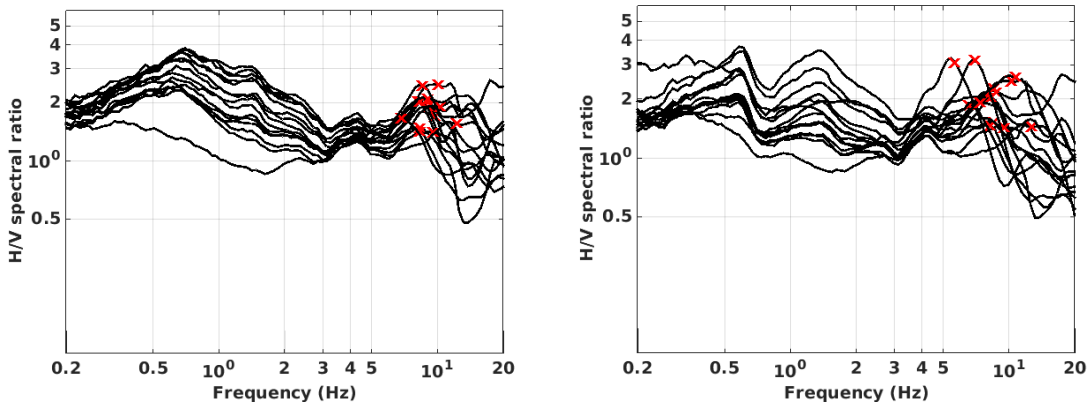

Figure 4: Comparison of H/V spectral ratios (time-frequency analysis code V. Poggi) between the different points of the arrays (left: MOE1, right: MOE2).

Moreover, all the methods to compute H/V ratios are compared at point MOE000 in Fig. 6, in which the classical methods were not divided by $\sqrt{2}$ (no correction for the Love wave contribution (Fäh et al., 2001)). The classical and TFA methods match well except that the amplitude of the TFA method of V. Poggi shows lower values (removal of Love waves) at high frequencies. The 3C FK analysis (Capon's method) of Poggi and Fäh (2010) matches with the H/V analysis below the fundamental frequency and shows lower amplitudes above.
The fundamental peak at the SMOE station is therefore at 10 Hz, with a peak amplitude of about 2.5.

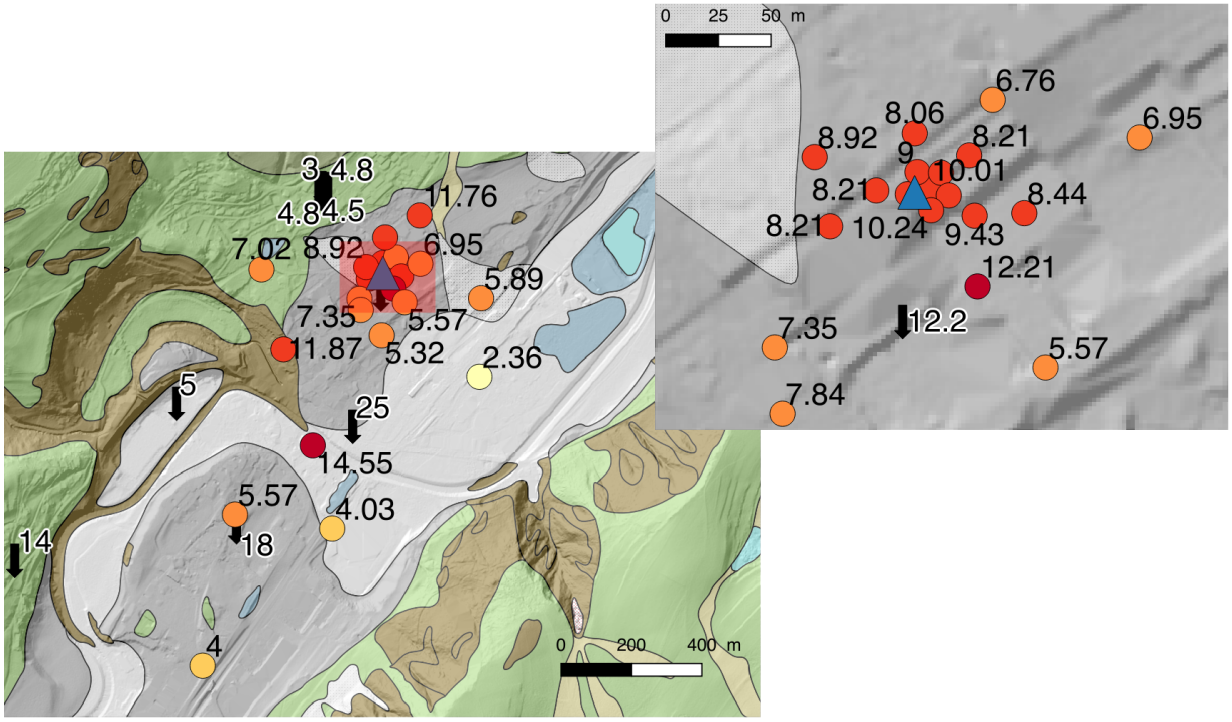

Figure 5: Maps of the identified peaks in the H/V ratios (frequency values in Hz) superimposed on the simplified geological map of the area (see Fig. 2 for the legend) and zoom around station SMOE. Boreholes (black arrows) with the depth value of the bedrock are also shown.

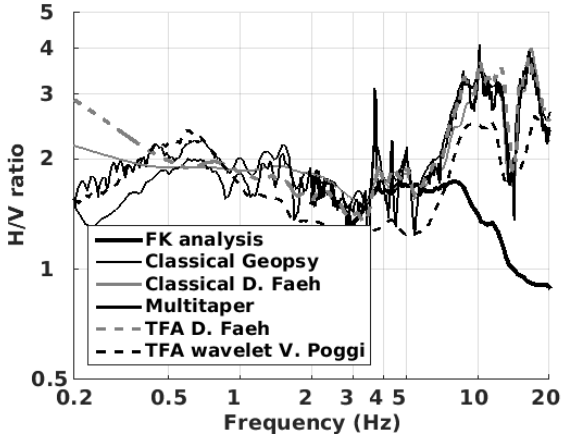

Figure 6: H/V spectral ratios for point MOE000 using the different codes. Classical methods were NOT divided by $\sqrt{2}$.

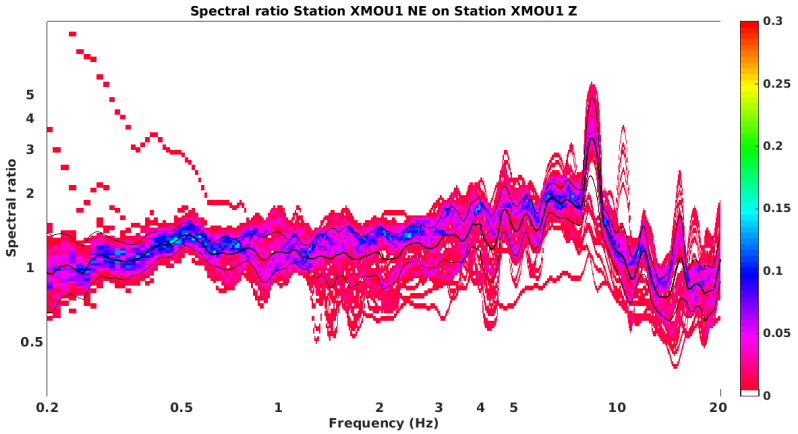

Figure 7: H/V ratios of temporary station XMOU1 located in the school area close to station MOE405.

3.2.2 Polarization analysis

A polarization analysis on the array data was performed to check for 2D resonance using the method of Burjánek et al. (2010). No particular polarization of the wavefield could be noticed across the array (Fig. 8). We assume therefore that there is no 2D resonance of the valley at this site.

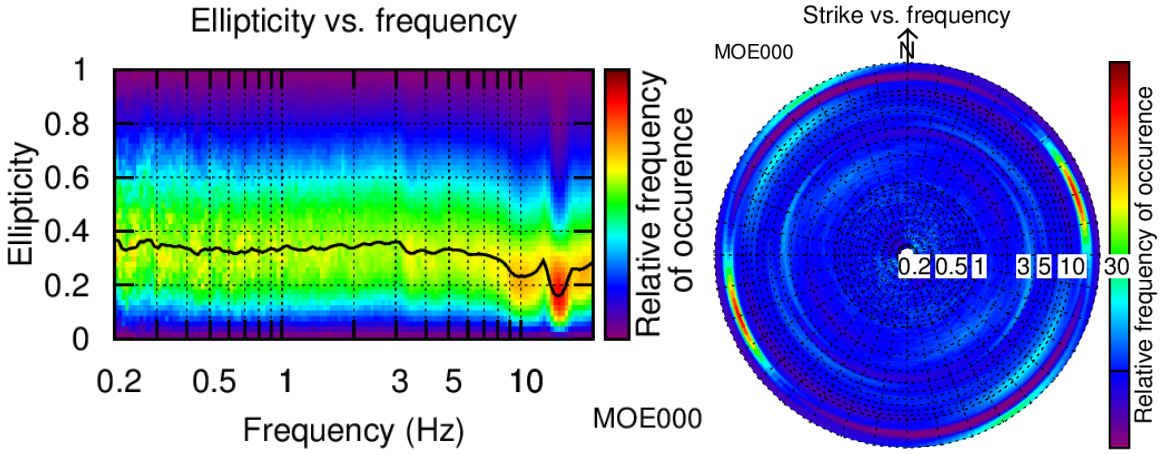

Figure 8: Polarization analysis at point MOE000. Left: Ellipticity (A trough in the ellipticity corresponds to polarized motion). Right: Strike of the polarization.

3.3 3-component high-resolution FK

The results of the 3-component high-resolution FK analysis (Poggi and Fäh, 2010) for the merged results of both configurations are shown in Fig. 9. The fundamental mode of Love waves is clearly determined from this analysis between 3.5 and 19 Hz (resolution limit: 4.1 Hz). The Rayleigh wave fundamental mode can be picked without discussion from the vertical component between 3.8 and 8.5 Hz. It can be noticed that for this frequency range, the energy on the radial component is shifted towards higher velocities as often the case. For higher frequencies, the picking is unclear, probably due to the lateral variations of the upper layers. We picked the Rayleigh wave from the configuration MOE2 (Fig. 10) because it gave better results during the inversion. It matches the radial component at high frequencies. The first higher mode is picked with some imagination from the vertical component.
The ellipticity curve determined with the 3-component HRFK analysis is described in the H/V analysis.

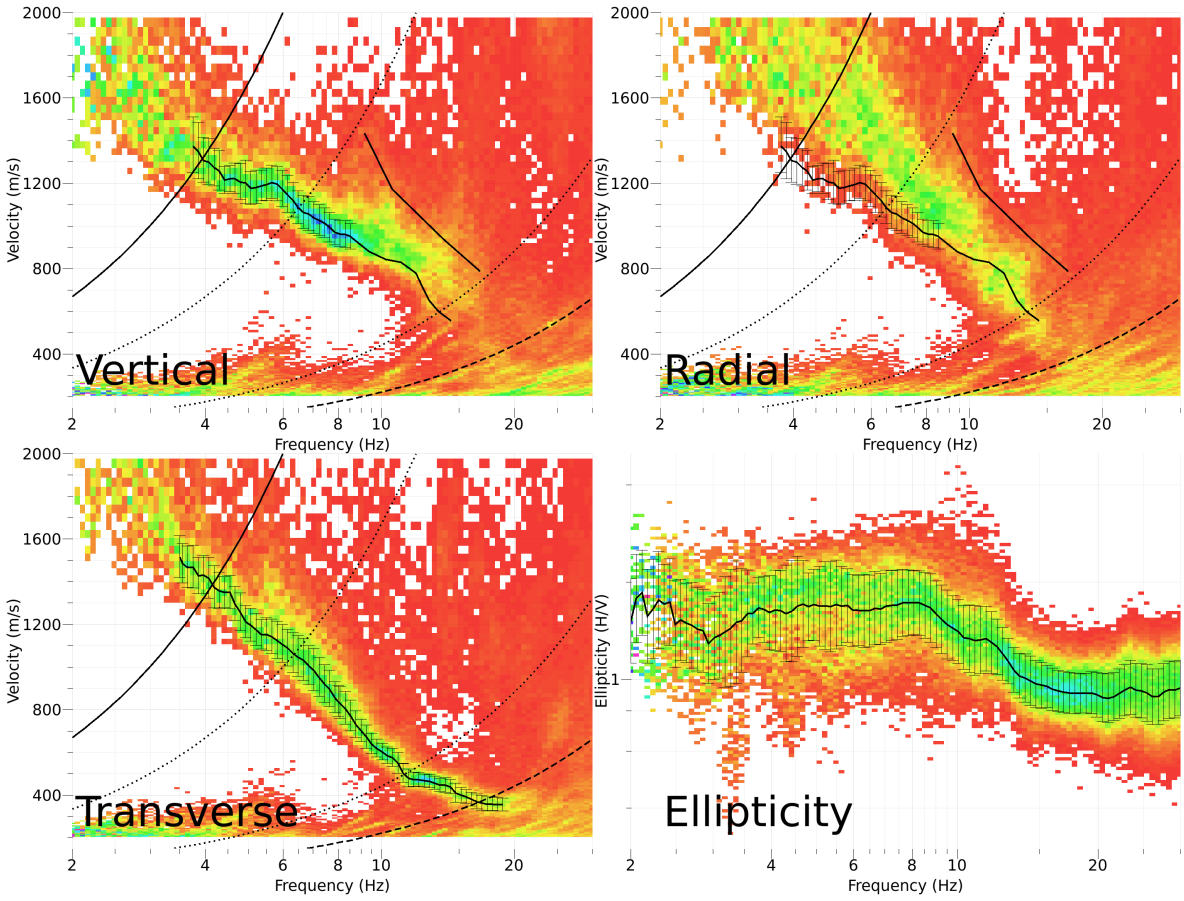

Figure 9: Dispersion curves obtained from the 3C HRFK analyses. The picking choices are described in the text.

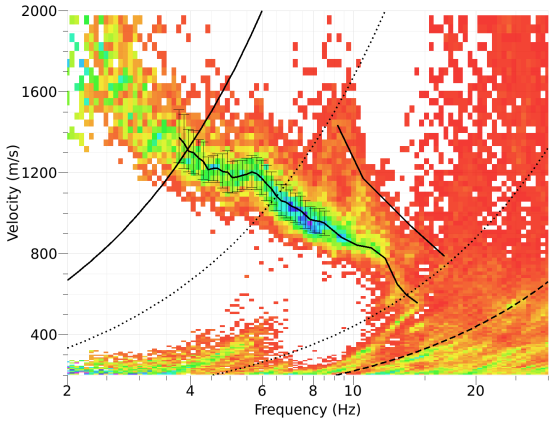

Figure 10: Dispersion curves obtained from the 3C HRFK analyses in the vertical component for dataset MOE2.

3.4 Wavedec

WaveDec (Maranò et al., 2012) has also been used to process the array data MOE2. This technique estimates the properties of multiple waves simultaneously with a maximum likelihood approach in the time domain. It was applied assuming the presence of 3 waves.
The fundamental Love and Rayleigh waves dispersion curves could be picked (Fig. 11) and are compared to the other analyses in section 3.5. The ellipticity of Rayleigh waves (Fig. 12) is relatively unclear but it seems that the sense of rotation changes at about 4 Hz (trough). The comparison with other proxys for the ellipticity curve (Fig. 6) is however not convincing.

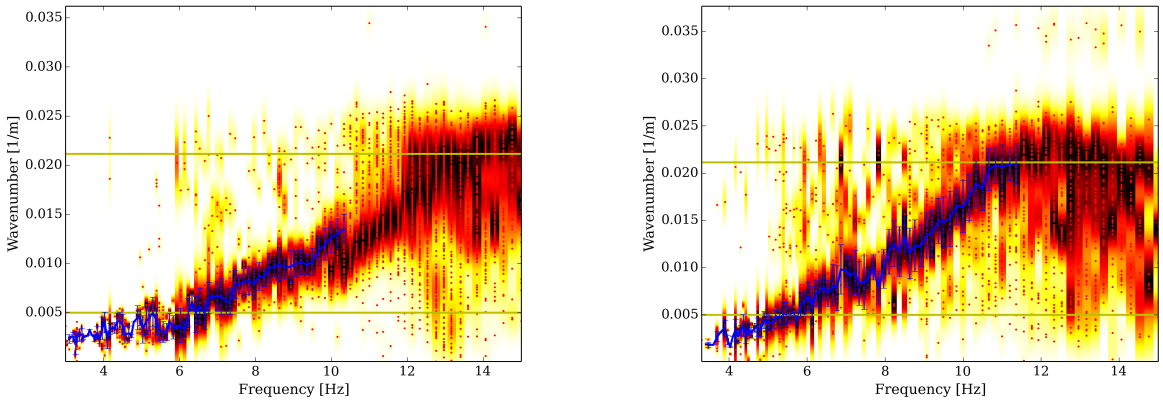

Figure 11: Rayleigh and Love wave fundamental dispersion curves obtained with the WaveDec technique (Maranò et al., 2012). The yellow lines indicate the theoretical array resolution limits.

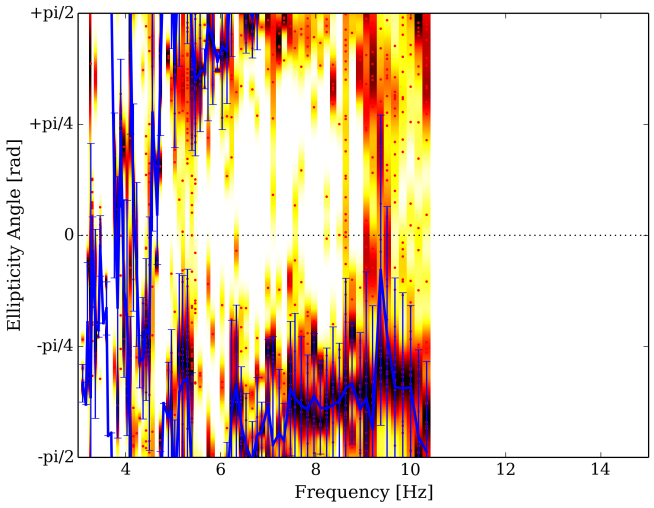

Figure 12: Rayleigh ellipticity angle curve obtained with the WaveDec technique (Maranò et al., 2012).

3.5 Interpretation

Fig. 13 gives an overview of the dispersion curves determined with the different methods. The curves are retrieved between 3.5 and 19 Hz with velocities ranging from about 1500 m/s at 3.5 Hz down to 350 m/s at 19 Hz for the fundamental Love mode. The results from WaveDec, though not smooth, agree with the 3C HRFK.

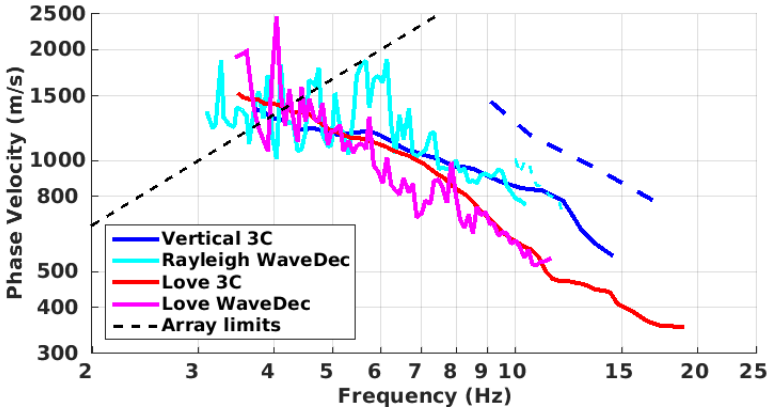

Figure 13: Picked dispersion curves from 3C HRFK analysis and the WaveDec method.

3.6 Data inversion

The inversion of the surface waves properties into 1D velocity profiles was performed using the Modified Neighborhood Algorithm (NA) (Wathelet, 2008) implemented in the Dinver software.

3.6.1 Misfit function

In the misfit function, the Rayleigh waves fundamental and first higher modes dispersion curves, the Love waves fundamental dispersion curve and the ellipticity curve above 6 Hz (H/V curve from the TFA code of V. Poggi at MOE000 point) were used as simultaneous targets without standard deviation. A low weight of 0.1 was assigned to the ellipticity curve. All curves were resampled using 50 points between 0.8 and 20 Hz in log scale.

3.6.2 Parametrization of the model space

The velocity was assumed to increase with depth. No velocity inversion is needed to explain the observed data. The Poisson ratio was inverted in each layer in the range 0.2-0.4 (no aquifer). The density was assumed to be 2000 kg/m^3 in the first layers and 2500 kg/m^3 in the rock layers. Inversions with free layer depths as well as fixed layer depths were performed. 4 layers are enough to explain most of the targets (dispersion and ellipticity), but more layers are used to smooth the obtained results and better explore the parameter space. 5 independent runs of 6 different parametrization schemes (4, 5 and 6 layers over a half space and 12, 12 and 13 layers with fixed depth) were performed, i.e. a total of 30 runs.

3.6.3 Results

Examples of retrieved ground profiles for these two strategies are presented in Fig. 14. When comparing to the target curves (Fig. 15), dispersion curves are generally well reproduced as well as the shape of the ellipticity. For further elaborations, the best models of these 30 runs were selected and used (see section 4.1).

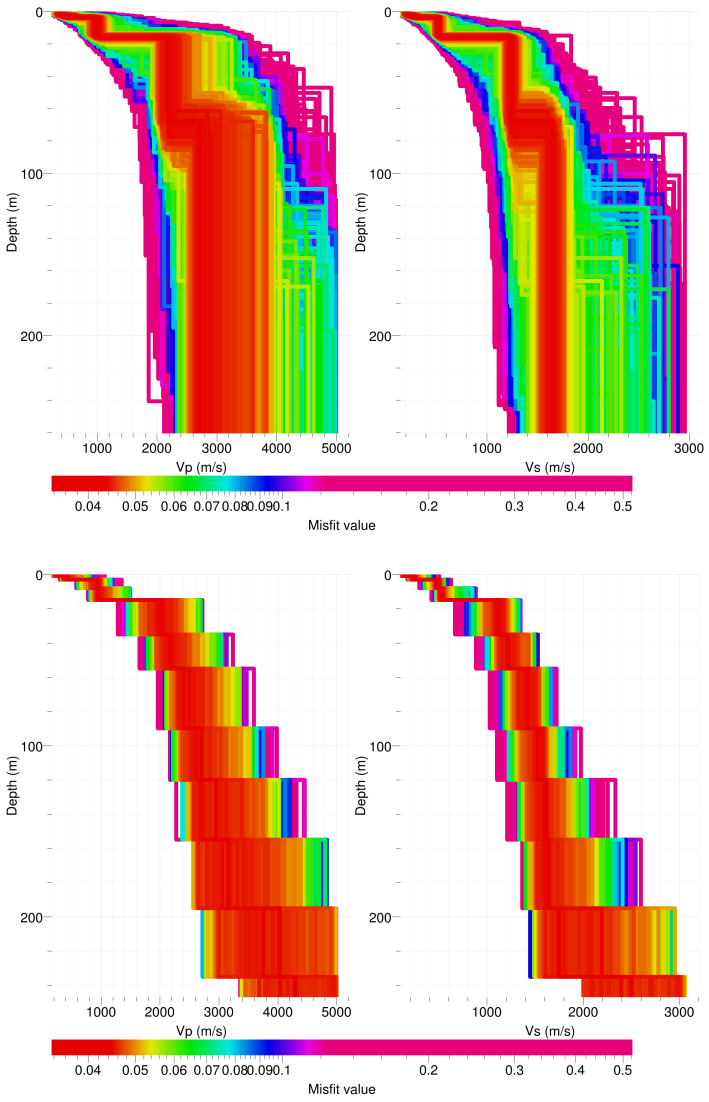

Figure 14: Inverted ground profiles at SMOE in terms of V_p and V_s for the first interpretation of Rayleigh waves; top: free layer depth strategy; bottom: fixed layer depth strategy.

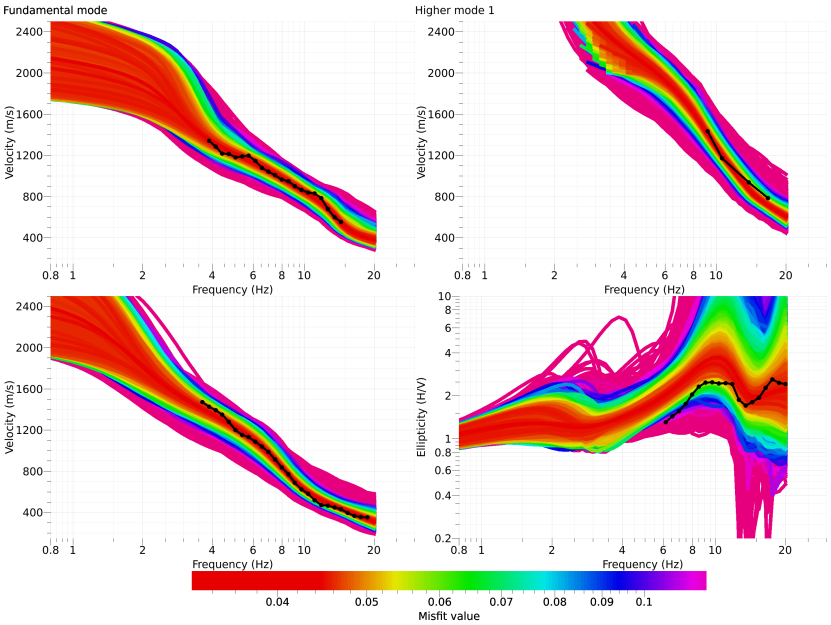

Figure 15: Comparison between inverted models and measured Rayleigh waves (top row fundamental mode: left, first higher mode: right) and Love waves (bottom row left) modes and corresponding ellipticity (bottom row, right) at site SMOE.

4 Interpretation of the velocity profiles

4.1 Velocity profiles

The first two to three meters of the profile show low velocities between 150 and 300 m/s. Below, a layer at about 530 m/s is found down to about 15 m. It corresponds to the "old" Quaternary alluvia and the moraine (not distinguishable), already well compacted considering the velocity. Their thickness is in accordance with the borehole data. The velocity contrast is strong with the underlying rock (Upper Marine Molasse) at about 1200 m/s. The velocity increases again at about 70 m depth up to 1600 m/s. It could correspond to the interface between the Upper Marine Molasse and the Lower Fresh Water Molasse, but more likely, it does not correspond to any geological interface. The velocity at greater depths than 200 m is not constrained.

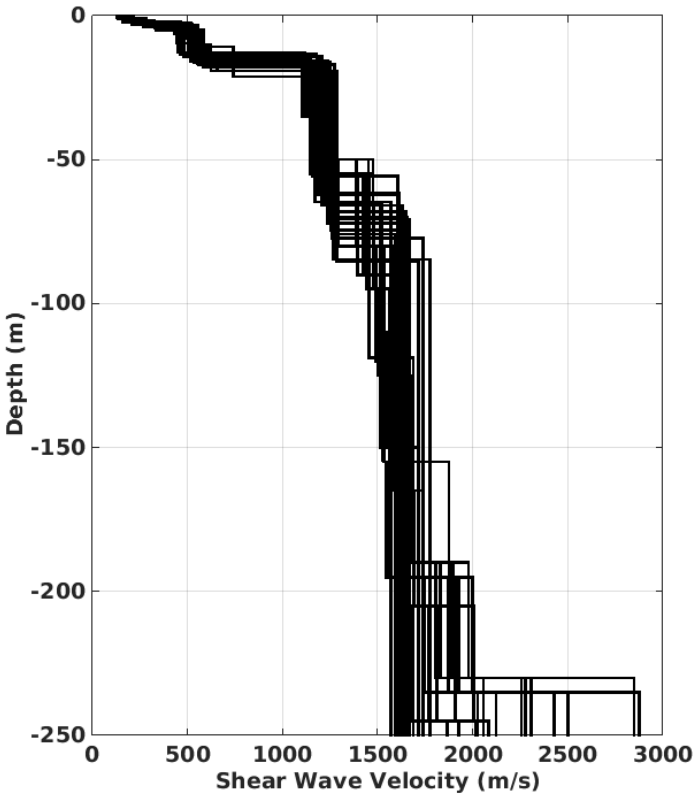

Figure 16: Shear-wave velocity profiles of the 30 selected models.

The distribution of the travel time average velocities at different depths was computed from the selected models. $V_{s,30}$ is found to be 582 m/s, corresponding to ground type B in the Eurocode 8 (CEN, 2004) and the SIA261 (SIA, 2014). However, it could be classified as type E in the SIA261 code if the upper sediments have a velocity lower than 500 m/s. This value is 530 m/s between 3 and 15 m, but 400 m/s on average over the 15 first meters. The thickness and velocity of the bedrock match with type E. Type E in the EC8 would require a velocity of the sediments of 360 m/s or lower. Finally the site can be classified as type E for SIA261, and type B for EC8.

4.2 Quarter-wavelength representation

The quarter-wavelength velocity approach (Joyner et al., 1981) provides, for a given frequency, the average velocity at a depth corresponding to 1/4 of the wavelength of interest. It is useful to identify the frequency limits of the experimental data (minimum frequency in dispersion curves at 3.6 Hz). The results using this proxy show that the dispersion curves constrain the profiles down to 50 m (Fig. 17). Moreover, the quarter wavelength impedance-contrast introduced by Poggi et al. (2012a) is also displayed in the figure. It corresponds to the ratio between two quarter-wavelength average velocities, respectively from the top and the bottom part of the velocity profile, at a given frequency (Poggi et al., 2012a). It shows a trough (inverse shows a peak) at the resonance frequency.

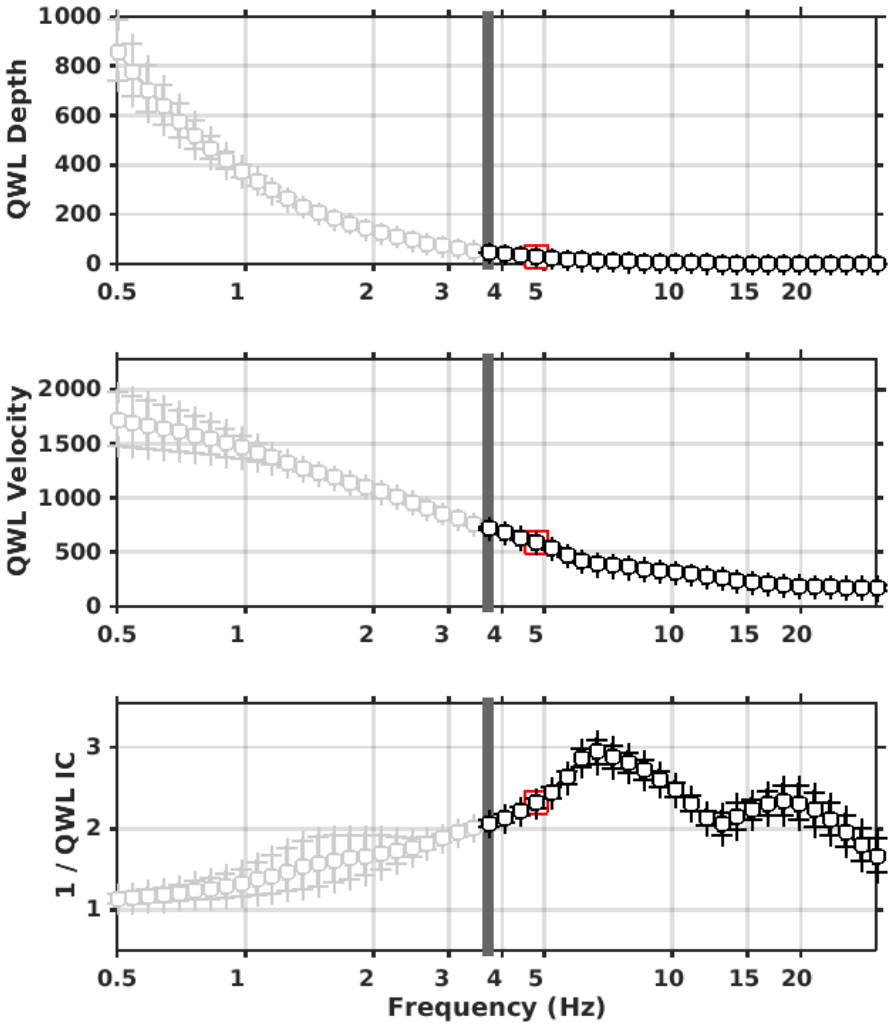

Figure 17: Quarter wavelength representation of the velocity profile for the selected velocity profiles (top: depth, center: velocity, bottom: inverse of the impedance contrast). The black curves are constrained by the dispersion curves, the light grey curves are not constrained by the data. The red square corresponds to V_{S30}.

4.3 SH transfer function

The theoretical SH-wave transfer function for vertical propagation (Roesset, 1970) is computed from the selected profiles. It is corrected with respect to the Swiss Reference Rock model (Poggi et al., 2011) following Edwards et al. (2013). It shows a peak at the fundamental frequency of resonance with an amplification of 3 (Fig. 18). It is compared to the amplification function obtained by empirical spectral modelling (ESM) (Edwards et al., 2013; Michel et al., 2014, 2016). The theoretical SH transfer function of the retrieved profiles matches the observed amplification function at station SMOE, although the amplitude at the peak is observed to be lower (factor of 2 instead of 3) (Fig. 18).

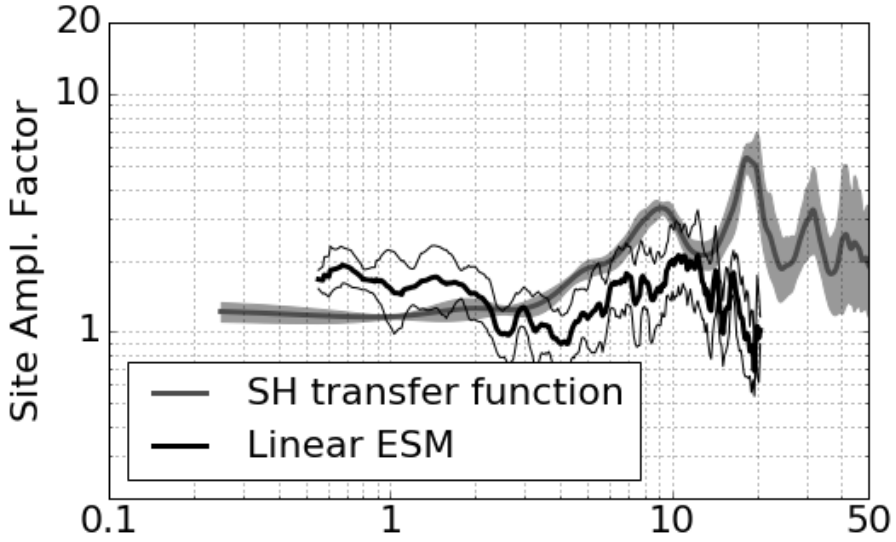

Figure 18: Comparison between the modeled SH transfer function for the selected velocity profiles and the empirical amplification (ESM) measured at station SMOE (with standard deviation).

5 Conclusions

The passive measurements presented in this study were successful in deriving a velocity model for the site SMOE. The soft sediment cover (old alluvia and moraine) is about 15 m thick with a low velocity over the 2-3 first meters and of about 530 m/s below. The rock located underneath (Upper Marine Molasse) has a velocity of about 1200 m/s. Another noticeable increase of velocity is found at about 70 m depth that may correspond to the interface with the Lower Fresh Water Molasse although it remains speculative. This report also presented an insight of the distribution of the sediment cover in the town. $V_{s,30}$ is 582 m/s and the site corresponds to ground type B in the Eurocode 8 (CEN, 2004) and type E in the SIA261 (SIA, 2014). The theoretical 1D SH transfer function computed from the inverted profiles shows an amplification of a factor of 2 to 3 at the resonance frequency of the soft sediment cover around 10 Hz.

Acknowledgements

The authors thank Dario Chieppa and David Farsky for their help with the array measurements.

References

Burjánek, J., Gassner-Stamm, G., Poggi, V., Moore, J. R., and Fäh, D. (2010). Ambient vibration analysis of an unstable mountain slope. *Geophysical Journal International*, 180(2):820–828.

CEN (2004). *Eurocode 8: Design of structures for earthquake resistance - Part 1: General rules, seismic actions and rules for buildings*. European Committee for Standardization, en 1998-1: edition.

Edwards, B., Michel, C., Poggi, V., and Fäh, D. (2013). Determination of Site Amplification from Regional Seismicity : Application to the Swiss National Seismic Networks. *Seismological Research Letters*, 84(4).

Fäh, D., Kind, F., and Giardini, D. (2001). A theoretical investigation of average H/V ratios. *Geophysical Journal International*, 145(2):535–549.

Joyner, W. B., Warrick, R. E., and Fumal, T. E. (1981). The effect of Quaternary alluvium on strong ground motion in the Coyote Lake, California, earthquake of 1979. *Bulletin of the Seismological Society of America*, 71(4):1333–1349.

Maranò, S., Reller, C., Loeliger, H. A., and Fäh, D. (2012). Seismic waves estimation and wavefield decomposition: Application to ambient vibrations. *Geophysical Journal International*, 191(1):175–188.

Michel, C., Edwards, B., Poggi, V., Burjánek, J., Roten, D., Cauzzi, C., and Fäh, D. (2014). Assessment of Site Effects in Alpine Regions through Systematic Site Characterization of Seismic Stations. *Bulletin of the Seismological Society of America*, 104(6):2809–2826.

Michel, C., Fäh, D., Edwards, B., and Cauzzi, C. (2016). Site amplification at the city scale in Basel (Switzerland) from geophysical site characterization and spectral modelling of recorded earthquakes. *Physics and Chemistry of the Earth, Parts A/B/C*.

Poggi, V., Edwards, B., and Fäh, D. (2011). Derivation of a Reference Shear-Wave Velocity Model from Empirical Site Amplification. *Bulletin of the Seismological Society of America*, 101(1):258–274.

Poggi, V., Edwards, B., and Fäh, D. (2012a). Characterizing the Vertical-to-Horizontal Ratio of Ground Motion at Soft-Sediment Sites. *Bulletin of the Seismological Society of America*, 102(6):2741–2756.

Poggi, V. and Fäh, D. (2010). Estimating Rayleigh wave particle motion from three-component array analysis of ambient vibrations. *Geophysical Journal International*, 180(1):251–267.

Poggi, V., Fäh, D., Burjánek, J., and Giardini, D. (2012b). The use of Rayleigh-wave ellipticity for site-specific hazard assessment and microzonation: application to the city of Lucerne, Switzerland. *Geophysical Journal International*, 188(3):1154–1172.

Roesset, J. (1970). Fundamentals of soil amplification. In Hansen, R. J., editor, *Seismic Design for Nuclear Power Plants*, pages 183–244. M.I.T. Press, Cambridge, Mass.

SIA (2014). *SIA 261 Einwirkungen auf Tragwerke*. Société suisse des ingénieurs et des architectes, Zurich, Switzerland.

Wathelet, M. (2008). An improved neighborhood algorithm: Parameter conditions and dynamic scaling. *Geophysical Research Letters*, 35(9):1–5.